Heliyon 6 (2020) e05821

Contents lists available at ScienceDirect

Heliyon

journal homepage: www.cell.com/heliyon

Review article

Controlled dispersion of ZnO nanoparticles produced by basic precipitation in solvothermal processes

Daniel Navas [a], Andrés Ibañez [b], Iván González [c], Juan Luis Palma [d,e], Paulina Dreyse [f,*]

[a] Departamento de Química, Facultad de Ciencias Naturales, Matemática y del Medio Ambiente, Universidad Tecnológica Metropolitana, Las Palmeras 3360, Ñuñoa, Santiago, 7800003, Chile
[b] Departamento de Física, Facultad de Ciencias Físicas y Matemáticas, Universidad de Chile, Av. Beauchef 850, Casilla 653, Santiago, Chile
[c] Facultad de Ciencias de la Salud, Universidad Central de Chile, Lord Cochrane 418, Santiago, Chile
[d] Center for the Development of Nanoscience and Nanotechnology (CEDENNA), Santiago, 9170124, Chile
[e] Engineering School, Universidad Central de Chile, Santa Isabel 1186, Santiago, 8330601, Chile
[f] Departamento de Química, Universidad Técnica Federico Santa María, Av. España 1680, Casilla 2390123, Valparaíso, Chile

ARTICLE INFO

Keywords:
Zinc oxide nanoparticles
Solvothermal treatment
Precipitation
Alkaline media
Ultrasonic cavitation
ZnO mesoporous

ABSTRACT

Zinc oxide nanoparticles were successfully synthesized under precipitation processes, using $ZnSO_4{\cdot}7H_2O$ as a Zn^{2+} precursor and K_2CO_3 used as a basic source, and hydrozincite was obtained as an intermediary, which was treated under two procedures; first procedure involved multiple stages to get final precipitated with NaOH, and in the second procedure the hydrozincite was straightforwardly dried at 220 °C. By both processes ZnO structures were obtained, which were turned into nanoparticles by a solvothermal treatment, for four hours in ethylene glycol at 200 °C. The final products for the first procedure was conglomerate of spherical nanoparticles with sizes ranged between 5–10 nm and dispersed ellipsoidal nanoparticles for the second procedure.

Apart off the two procedures mentioned above, another synthesis was carried out with the same Zn^{2+} precursor but now using NaOH, and the solvothermal treatment produced ZnO mixed micro-structures which under ultrasonic cavitation disaggregated on mesoporous ZnO nanoplates of hexagonal shapes with nanopore sizes of approximately 0.35 nm. All ZnOs synthesized were structurally characterized with XRD, TEM and FT–IR techniques, and electronically with UV–Vis absorption and diffuse reflectance spectroscopies.

1. Introduction

In recent decades, Zinc oxide has attracted attention in many application fields based on its nanomaterials, specifically its nanoparticles (ZnO NPs) [1, 2, 3, 4, 5, 6] and one-dimensional (1–D) nanostructures such as nanotubes, nanoclips, nanowires and nanorods [7, 8, 9, 10]. The synthetic routes of nanomaterials involve many physical and chemical parameters that directly influence the size, shape, morphology and conglomeration-dispersion [11, 12, 13, 14, 15]. In this regard, a wide variety of Zn^{2+} salts have been used as precursors in basic media to produce ZnO NPs under precipitation methods [16]. The $ZnSO_4{\cdot}7H2O$ salt stands out for being low cost, easily soluble in water and suitable for many syntheses methods without other pretreatments [17, 18, 19]. Concerning the basic media, the Zn^{2+} precursors have been reacted with aqueous solutions of strong bases (NaOH, LiOH and KOH), tuning the morphology of the nanoparticles in different ways [20, 21, 22, 23, 24, 25, 26], or using weak bases (NH_4OH, urea and Na_2CO_3) to generate outstanding achievements in morphology, size distribution and dispersion [27, 28, 29].

The synthesis of ZnO in alkaline media is strongly dependent on the Zn^{2+}/OH molar adjustment [30]. As literature described, with a 0.5 M ratio of $ZnSO_4$/NaOH, the $Zn(OH)_2$ precipitate first originates rapidly and is then converted to ZnO by a hydroxide catalyzed process; if the molar ratio is below 0.5, basic zinc sulfate is precipitated, while no precipitate forms if there is not enough base to raise the pH (>12) [31]. Although pH is a determining factor to produce ZnO NPs, it should be taken into account that the intrinsic characteristics, that is, morphology and yield also depend on parameters such as temperature, reaction time and mixing procedures of the initial reagents.

To obtain ZnO NPs with homogeneous morphologies and tuned size distributions, the solvothermal and hydrothermal processes have proven to be successful [32]. Generally, these treatments have been carried out

* Corresponding author.
E-mail address: paulina.dreyse@usm.cl (P. Dreyse).

https://doi.org/10.1016/j.heliyon.2020.e05821
Received 8 September 2020; Received in revised form 1 November 2020; Accepted 18 December 2020

using autoclave systems with different salts of Zn^{2+} mixed with alcoholic solvents, water, and usually aided with organic templates as surfactants at temperatures between 100-350 °C [33, 34, 35, 36, 37]. Thus, new morphologies and structures are achieved under controlled pressure and temperature, which are not usually feasible to obtain at room temperature. The type of solvent in these treatments also affect the ZnO NP shapes as has been reported by *Goshal et al.* [38], using mixtures of ethylene glycol (EG) and ethanol, producing a gradual change in the shape nanoparticles from ellipsoidal to spherical, while increasing the volume of EG, since this solvent acts as a stabilizing agent, restricting the growth and suppressing the NPs agglomerations [39]. Furthermore, EG reduces the diffusion rate Zn^{2+} ions helping the small NPs production since it has a high viscosity and weaker ionic strength compared to water [40].

On the other hand, another approach to produce ZnO NPs involve the conversion of micrometric size into smaller dimensions under ultrasonic irradiation, due to nucleation and crystal growth on established ZnO microparticles, resulting in new granular surfaces and reproducible nanostructures [41]. The phenomenon responsible is cavitation, in which liquids are rupture and form vapor bubbles if the liquid pressure is decreased beyond a critical tension. Ultrasonic cavitation is very effective in breaking particle agglomerates. The shock force that takes place during the cavitation process, added to high local temperatures, can break the nanoparticle clusters, therefore, the dispersion obtained is the consequence of micro-turbulence caused by fluctuations of pressure and cavitation [42, 43]. For example, this process has been used in ZnO NPs modification with Mg^{2+} ions under strong sonication to tune the band gap amplitude [44]. *Sharifalhoseini et al.* [45] used the ultrasonic cavitation to improve the morphology of the ZnO nanostructure, applying direct (high intensity in a horn system) and indirect sonication (low intensity ultrasonic bath) yielded flowers and stars nanoparticles, respectively.

Considering the above mentioned, we study precipitation methods to produce ZnO NPs by solvothermal treatment enhancement, focusing on the influence of the basic strength of the precipitating agents. Three syntheses were evaluated to improve the ZnO NPs dispersion, using $ZnSO_4{\cdot}7H_2O$ as Zn^{2+} precursor and NaOH or K_2CO_3 as precipitating agents. Synthesis I involved the precipitation with NaOH, originating ZnO microstructures. On these structures, ultrasonic irradiation was applied to turn the micrometric phase into nanometric structures, producing nanoporous hexagonal grating nanoplates. In synthesis II the precipitation was carried out with K_2CO_3, by several intermediary reactions, producing ZnO which under solvothermal treated, yielded small spherical ZnO NPs in agglomerations. Synthesis III also involved K_2CO_3 but avoiding some intermediate steps concerning to the second route, producing ellipsoidal ZnO NPs without agglomerations.

The ZnO structures were fully characterized by spectroscopic techniques (X-Ray diffraction, FT-IR, reflectance and UV-Visible absorption) and by TEM microscopy, confirming the size and distribution in each case, highlighting the small ZnO NPs from the second and third synthesis in promising applications as semiconductors [4, 46, 47]. As well as the nanostructures produced from ultrasonic cavitation endowing the nanomaterials with a high degree of porosity [48], enhancing their reactivity for catalysis [49], energy conversion [50, 51], among other types of applications [52].

2. Experimental procedures

2.1. Reagents

All reagents were purchased from Merck and Sigma-Aldrich and were used without further purification; nanopure water was used in every procedure required.

2.2. Zinc oxide precursors synthesis

2.2.1. Synthesis I

25 mL of 0.050 M aqueous solution of $ZnSO_4{\cdot}7H_2O$ were stirred and heated in a round bottom flask. Once the temperature was raised to 80 °C, 25 mL of 0.10 M aqueous NaOH solution were added under constant stirring. The mixture was kept four hours under constant stirring and temperature (80 °C). The white precipitate obtained was centrifuged, washed several times with water and dried at 220 °C for six hours in an oven.

2.2.2. Synthesis II

In the same way as in the first synthesis, the Zn^{2+} precursor solution (25 mL of $ZnSO_4{\cdot}7H_2O$ 0.050 M) was stirred and heated to 80 °C, then 25 mL of 0.15 M aqueous K_2CO_3 solution were added under constant stirring. During four hours, the mixture was kept under stirring at 80 °C and a white precipitate was observed. It was filtered, washed several times with water and dried at 80 °C. Then, 25 mL of 7.0 M aqueous acetic acid solution were added, and the mixture was stirred for 15 min; then, the solvent was removed by evaporation. The obtained solid was dissolved in 50 mL of an ethanol/water (1:1) mixture and precipitated using 25 mL of 0.10 M NaOH. The white solid precipitate was centrifuged and washed with deionized water several times and was dried at 220 °C for six hours in an oven.

2.2.3. Synthesis III

It was carried out in the same way as the first stage (K_2CO_3 precipitation) of the second synthesis, and the filtered and washed white precipitate was straightforwardly treated at 220 °C in an oven for six hours.

2.3. ZnO NPs by solvothermal treatment

Each of the solids obtained in the previous syntheses were suspended separately in an EG:water (10:1.0 mL) mixture in a round bottom flask and kept under constant stirring at 80 °C; then, the suspension was transferred to a stainless steel reactor and treated with solvothermal synthesis for six hours at 200 °C. The obtained nanoparticles were cleaned several times with water and acetone and dried at 80 °C.

2.4. Bath and probe ultrasonic treatments

In the case of the first synthesis (considering solvothermal treatment), ZnO microstructures were obtained, therefore, to disaggregate these microstructures into nanoparticles, ultrasonic treatments were applied using bath processes and an ultrasonic probe.

For the bath, three separately ethanol-suspension samples were ultrasonically irradiated for 15, 30 and 60 min, respectively. For ultrasonic probe processes, three separately ethanol-suspension samples were treated for 30, 60 and 90 min, respectively.

2.5. Characterization techniques

The structural characterization of all samples was performed using a SIEMENS D 5000 X – Ray diffractometer (Cu Kα, $\lambda = 1.5418$ Å, operation voltage 40 kV, current 30 mA). Fourier transform infrared (FT-IR) spectra of all samples were measured using a Jasco FT/IR – 4600 equipment in the region of 4000–400 cm^{-1}, from samples prepared in KBr pellets. Characterization by UV-Vis spectroscopic was performed using a Thermo Scientific evolution 220 model spectrophotometer; all UV–Vis absorption spectra were recorded for different ZnO samples in ethanol, in a range of 210–750 nm. Band gaps from each ZnO powders were determined using diffuse reflectance UV-Vis spectra recorded between 200-800 nm, at 200 nm/min scan rate using a Jasco V-750 spectrophotometer with an integrating sphere (Spectralon reference tile cap). Reflectance measurements

were transformed to absorption spectra using the Kubelka-Munk function. Morphological characterization was carried out with a Hitachi HT7700 high-resolution transmission electron microscope. All samples were previously suspended in absolute ethanol and dropped on a TEM grid and left to dry at room temperature.

3. Results and discussion

3.1. Synthetic procedures of intermediates and final products

The three synthetic routes performed to obtain ZnO were successfully carried out. The ZnO obtained from the first and second routes was washed with deionized water to remove some impurities and then was dried at 220 °C. In the case of the third route, the heating of hydrozincite at 220 °C straightforwardly provided the formation of ZnO.

In synthesis I, the precipitation process started immediately when NaOH was added to the Zn^{2+} solution. According to the literature, the precipitated white powder corresponds in a first stage to $Zn(OH)_2$ intermediate, but as soon the pH increases, it becomes ZnO [53, 54, 55, 56]. The general reaction of this synthetic procedure can be described by the following equation:

$$ZnSO_4 \cdot 7H_2O_{(ac)} + 2NaOH_{(ac)} \rightarrow \boldsymbol{ZnO}_{(s)} + Na_2SO_{4(ac)} + 8H_2O_{(l)}$$

In this synthesis it is proposed that $Zn(OH)_2$ would have undergone a fast phase transformation into ZnO during the precipitation process which is supported by at least three mechanisms that could explain this transformation: dissolution-reprecipitation, in situ crystallization and/or transformation of solid–solid phase; all of them have been observed for example, throughout the synthesis stages of ZnO hydrothermal microflowers [57].

Synthesis II was carried out with K_2CO_3 and Zn^{2+} solutions obtaining hydrozincite ($Zn_5(CO_3)_2(OH)_6$) as a product, which stoichiometrically blends $Zn(OH)_2$ and $ZnCO_3$ in a 3:2 ratio. Then, the hydrozincite was treated with acetic acid producing the precursor of $Zn(CH_3COO)_2$, turning carbonate anion into carbon dioxide and also solubilizing $Zn(OH)_2$. The following equations are proposed to represent the chemical processes in accordance with the X-Ray diffractograms obtained (*vide infra*).

$$5ZnSO_4 \cdot 7H_2O_{(ac)} + 5K_2CO_{3\ (ac)} \rightarrow \boldsymbol{Zn_5(CO_3)_2(OH)_{6\ (s)}} + 3CO_{2\ (g)} + 5K_2SO_{4\ (ac)} + 32H_2O_{(l)}$$

$$\boldsymbol{Zn_5(CO_3)_2(OH)_{6\ (s)}} + 10CH_3COOH_{(ac)} \rightarrow 5\boldsymbol{Zn(CH_3COO)_2 \cdot 2H_2O_{(ac)}} + 2CO_{2\ (g)} + 6H_2O_{(l)}$$

The next stage involved hydrolysis of $Zn(CH_3COO)_2$ in ethanol/water adding NaOH. This process might incorporate many chain reactions leading ZnO formation. A zinc acetate complex [$Zn_4O(CH_3COO)_6$] could probably be obtained and then produced a $Zn_5(OH)_8(CH_3COO)_2$ intermediary, which decomposes to ZnO as pH increases [58]. Two main chemical reactions can be related to this process, namely: (1) hydrolysis; where zinc acetate complexes react with NaOH, originating tetrahedral zinc hydroxide complexes with different coordination $[Zn(OH)_n]^{2-n}$, and (2) condensation; where zinc hydroxide complexes react again with zinc acetate complexes generating Zn – O – Zn bonds [59]. The following equations are suggested to represent ZnO formation as was identified by X-Ray experiments.

$$5\boldsymbol{Zn(CH_3COO)_2 \cdot 2H_2O_{(ac)}} + 8NaOH_{(ac)} \rightarrow \boldsymbol{Zn_5(OH)_8(CH_3COO)_2 \cdot 2H_2O_{(ac)}} + 8CH_3COONa_{(ac)}$$

$$\boldsymbol{Zn_5(OH)_8(CH_3COO)_2 \cdot 2H_2O_{(ac)}} \rightarrow 5\boldsymbol{ZnO}_{(s)} + 2CH_3COOH_{(ac)} + 5H_2O_{(l)}$$

Synthesis III was carried out in the same way as the previous synthesis but avoiding multiple steps. That is, by mixing CO_3^{2-} and Zn^{2+}, hydrozincite was also obtained, which straightaway turned into ZnO during the drying process at 220 °C. This behavior allows us to suggest a possible decomposition of hydrozincite, as previously identified by differential thermogravimetric analyses for the solid phase transformation of $Zn_5(CO_3)_2(OH)_6$, where the main mass loss occurred at 220 °C due to a simultaneous decomposition of $ZnCO_3$ and $Zn(OH)_2$ [60]. According to this description, the equations shown could then summarize the third synthesis route performed.

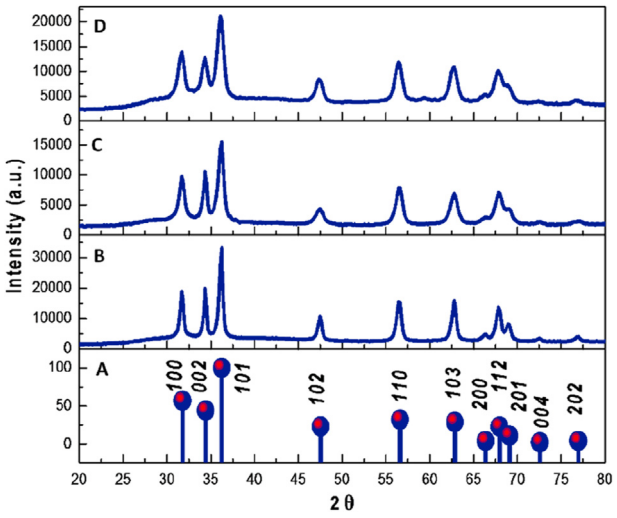

Figure 1. X-Ray diffraction of the ZnO obtained from A. Zincite PDF 36–1451 and synthesis: B. I, C. II and D. III.

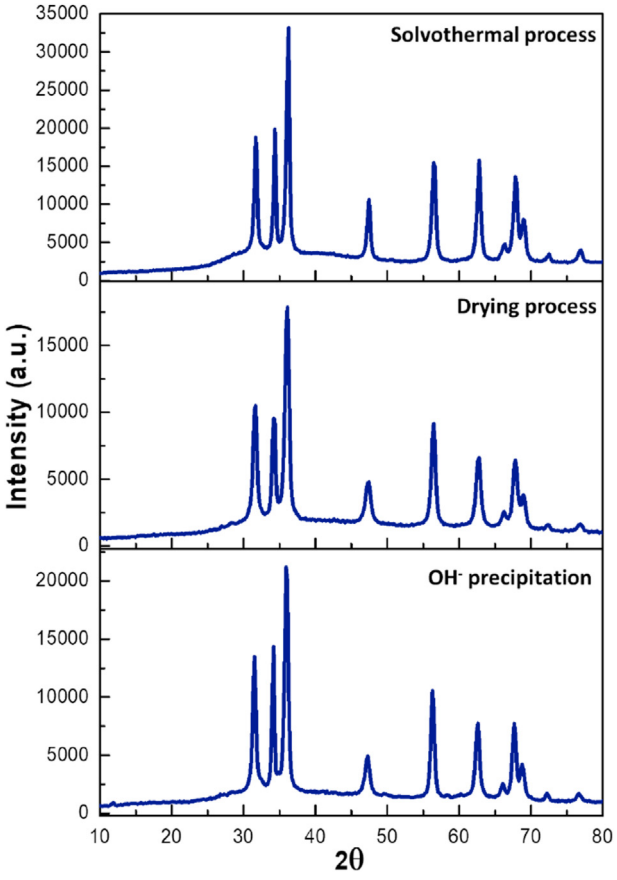

Figure 2. X-Ray diffraction of the ZnO obtained from synthesis I.

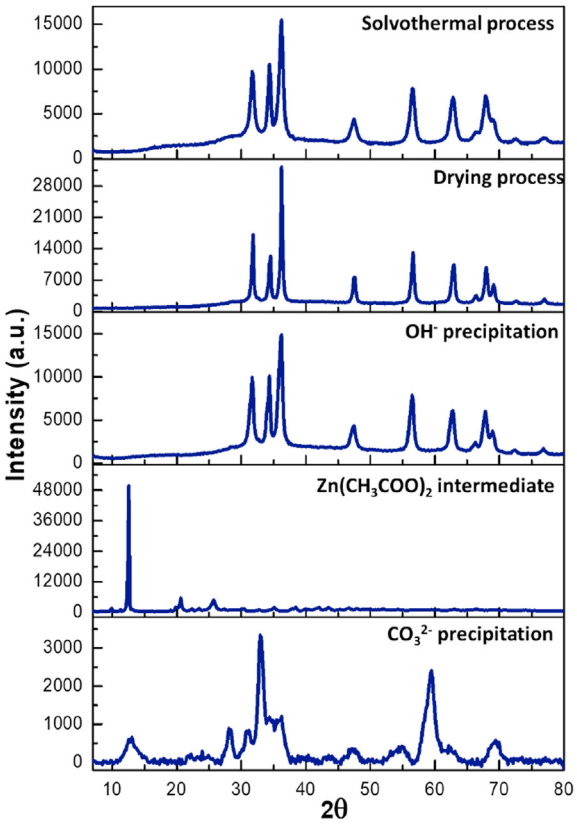

Figure 3. X-Ray diffraction of the ZnO obtained from synthesis II.

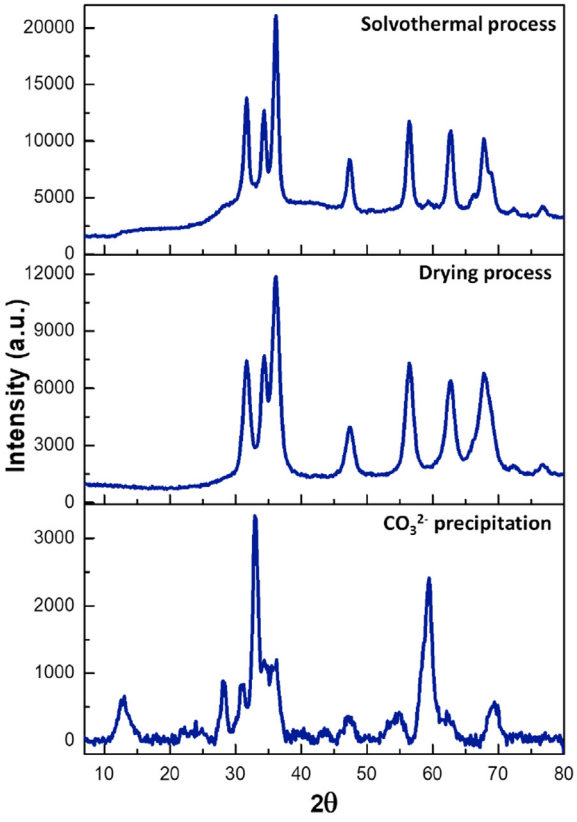

Figure 4. X-Ray diffraction of the ZnO obtained from synthesis III.

$$5ZnSO_4 \cdot 7H_2O_{(ac)} + 5K_2CO_{3\ (ac)} \rightarrow \boldsymbol{Zn_5(CO_3)_2(OH)_{6\ (s)}} + 3CO_{2\ (g)} + 5K_2SO_{4\ (ac)} + 32H_2O_{(l)}$$

$$\boldsymbol{Zn_5(CO_3)_2(OH)_{6\ (s)}} \xrightarrow{\Delta} 5\boldsymbol{ZnO}_{(s)} + 2CO_{2\ (g)} + 3H_2O_{(g)}$$

Zinc oxides obtained by the three syntheses described were subsequently undergone to solvothermal treatments to yield ZnO NPs. Before the treatment, all samples were suspended and heated at 80 °C in an EG/water mixture, to suppress and control the crystal growth in the solvothermal stage and to facilitate ZnO dispersion. Solvothermal treatment was the final stage in each synthetic route, where temperature, time and pressure were the key factors to induce the formation of nanoparticles in the case of synthesis II and III. Conversely, from the synthesis I ZnO microstructures were obtained.

3.2. Characterization by powder X-Ray diffraction

The X-Ray diffractograms of ZnO samples obtained from the solvothermal processes in the three synthetic routes are compared in Figure 1. Here, similar XRD patterns corresponding to the zincite phase are observed compared to PDF 36–1451. The three diffractograms agree with the hexagonal wurtzite structure with $a = 3.250$ Å and $c = 5.207$ Å lattice parameters [46]. As can be seen, no other crystalline peaks related to other phases of zinc oxide were found, confirming that all synthesis routes provide the desired ZnO. Concerning to the peak intensities, the diffractogram of synthesis I exhibits the highest intensities in contrast with C and D diffractograms, therefore, in synthesis II and III the ZnO structures formed might have sustained size decrease, suppressing crystal growth to yield nanostructures.

Figures 2, 3, and 4 show all diffractograms obtained from the three synthetic routes at every single stage. Figure 2 corresponds to X-ray diffractograms associated with Zn^{2+} straightforward precipitation with NaOH (synthesis I). All recorded XRD patterns are the same, confirming that the ZnO hexagonal wurtzite lattice (PDF 36–1451) is preserved throughout the whole process. Also, an interesting featuring is observed in the peak at 36.039 (2θ) which substantially increases at each stage, which may be related to crystal growth of the ZnO structure which is concomitant to plane *101*.

The diffractograms of synthesis II are shown in Figure 3. The first stage of precipitation (Zn^{2+} and K_2CO_3) results in hydrozincite, since the lattice parameters are related to the monoclinic cell centered with $a = 13.58$ Å, $b = 6.280$ Å and $c = 5.410$ Å, accordingly to PDF 19–1458 (see Figure S1 in supplementary data). The second stage exhibits $Zn(CH_3COO)_2$ reflections (PDF 01–0089) without specific lattice assignments, suggesting the presence of zinc acetate intermediaries layers. The third (NaOH addition) and fourth (solvothermal treatment) stages show diffractograms very similar among them and similar to Figure 2, therefore, the signals are attributed to ZnO wurtzite lattice.

In the first stage for synthesis III (Figure 4), the diffractogram exhibits a structural phase of hydrozincite. In the second stage (drying process), the precursor shifted to ZnO, showing the hexagonal structure of the wurtzite. This behavior could be associated with a substantial amount of hydrozincite should have decomposed through drying process at 220 °C. Here, wide reflection peaks are observed, suggesting a mixture of ZnO nanostructures and/or some absorbed carbonate anion. The third stage exhibits a similar ZnO wurtzite lattice compared to the other solvothermal synthetic routes; however, the widening peaks withdraws considerably suggesting a change of ZnO morphology obtained by this synthesis compared to the others.

To confirm whether the widening of the peaks is due to the excess carbonate used (1.0:3.0 mol ratio of Zn2+/CO32-), another synthesis was performed using less excess carbonate (1.0:1.2 of Zn2+/CO32-). The obtained diffractogram patterns (see Figure S2 in supplementary data) were the same compare to those obtained using high excess carbonate, indicating that residual carbonate is a consequence of the synthesis itself

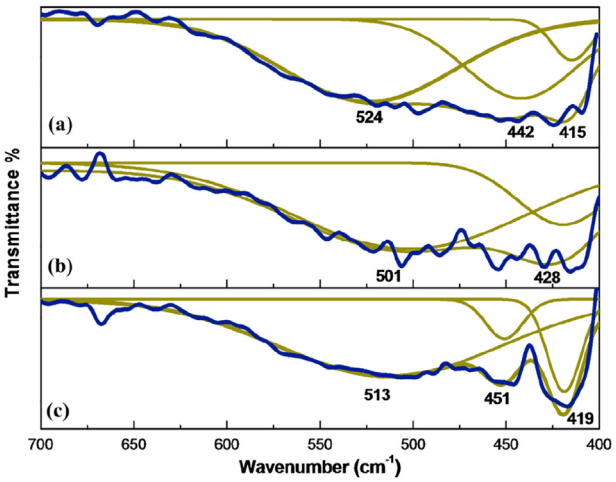

Figure 5. FT-IR spectra (short wavenumber scale) of ZnO obtained after solvothermal treatment from synthesis: (a). I, (b) II and (c) III. Original spectra (blue lines) and deconvolution spectra (green lines).

and not from the amount of carbonate used. A possible explanation could be related to the temperature used to promote hydrozincite decomposition which may be insufficient to allow the conversion of all CO32-.

3.3. Vibrational and electronic characterizations

The short-wavenumber scale FT-IR spectra of ZnO obtained are exhibited in Figure 5. The long scan (4000–400 cm^{-1}) spectra are depicted in supplementary data (Figure S3). The 400–1000 cm^{-1} region presents the ZnO characteristic IR absorption peaks. The three spectra were deconvoluted to identify the Zn–O vibrations, displaying the same features in the region from 400 to 600 cm^{-1}; the strong bands observed around ~420 and 447 cm^{-1} correspond to Zn–O vibrations, similar to the reported FT-IR spectra of ZnO NPs [61]. The broad band ~514 cm^{-1} could be associated with oxygen deficiency and/or oxygen vacancy (OV) defect complex in ZnO [62]. Additionally, some ZnO vibrational modes appeared to be shifted accordingly with the synthetic route used. Since every bond in ZnO NPs have some different strength degree, mixed wide band vibrations are a consequence of this unusual kind of bonds at nanometric scale [45].

On the other hand, UV–Vis spectra were recorded for ZnO structures and shown in Figure 6. All spectra show a maximum absorption peak relates to the large exciton binding energy of ZnO NPs [63, 64]. These peaks are registered at 373, 363 and 360 nm for synthesis I, II and III, respectively. In the spectrum obtained from synthesis III, in the wavelength region of 200–360 nm, a different absorption profile can be observed compare to another two spectra. Since carbonate anion has absorption at this wavelength [65], this feature could be attributed to presence of residual carbonate, as it was explained in the X-Ray diffractogram of this sample, in relation to wide peaks observed. Furthermore, another interpretation might be attributed to effect of quantum confinement for small nanocrystals, which originates the excitonic absorption band located in between 260-267 nm [66].

The absorption peak of the bulk ZnO should be recorded around 385 nm, therefore, considering the blue shift of all the spectra shown, the synthesized ZnO particles could be in the quantum regime [67].

The absorption red – shifted of the ZnO obtained from synthesis I in comparison with the absorptions obtained from synthesis II and III, could be indicate the presence of microstructures as described in detail in TEM section. In order to identify the optical band gaps of the samples, diffuse reflectance studies in the UV – Vis region were carried out in solid state, since the optical band gap values can be extracted from powder semiconductors without any ambivalence [68]. Figure S4 of the supplementary data exhibits the $[F(R)h\nu]^2$ vs photon energy graphs from each ZnO NPs synthesis. The calculated optical band gaps in all cases are around 3.20 eV, evidencing the band gap decline compare to bulk ZnO which averages 3.4 eV [69]. This behavior is attributed to lattice structural atom-packing defects that are featured in the powder; these intrinsic defects are associated to negative and positive oxygen vacancies, that are located approximately ≈0.2 eV below the conduction band according to literature [70]. In our case this might be related to synthesis procedures and conditions, considering that the different stages performed since the precipitation, the surfactant templates absence, drying processes and solvothermal treatment could have contributed some lattice defects sources during the growth process originating a higher level of surface oxygen vacancies as a consequence of higher surface area to volume ratio for smaller NPs [71, 72].

Considering that the nanometric sizes from the absorption and reflectance measurements are not corroborated, TEM experiments show conclusive evidence of the ZnO NPs produced by syntheses II and III as described in the next section.

3.4. Characterizations by transmission electron microscopy (TEM)

TEM images of the ZnO structures obtained from the three syntheses are depicted in Figure 7 with the corresponding histograms to designate one or two dimensions (length: L and W: wide) according to the shape of the ZnO structure analyzed.

From synthesis I (Figure 7 (a)), TEM images show ZnO microstructures without a defined morphology were obtained. In particular, the Figure exhibits two microstructures that might have been formed through a nanorods self-assembly mechanism, generating multi-size blending structures aligned through the *101* plane direction. Probably, in this synthesis the sizes and morphologies of the structures differ to small a degree throughout the process, since from the precipitation stage a tendency of morphology elongation is adopted, on a scale of micrometric size, accordingly to TEM images before the solvothermal process (see Figure S5 in supplementary data). Therefore, this synthesis yields ZnO microstructures in the first stage due to a fast transformation from $Zn(OH)_2$ to ZnO aided with NaOH, where apparently solvothermal treatment offers a minimum advantage for nanoparticles formation.

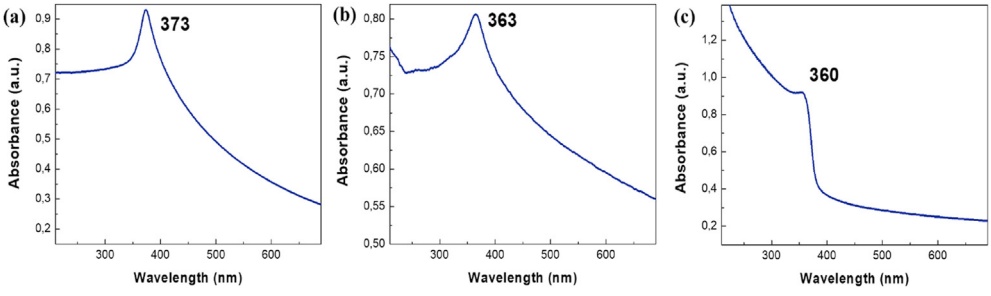

Figure 6. UV-Vis absorption of ZnO NPs from synthesis: (a) I, (b) II and (c) III.

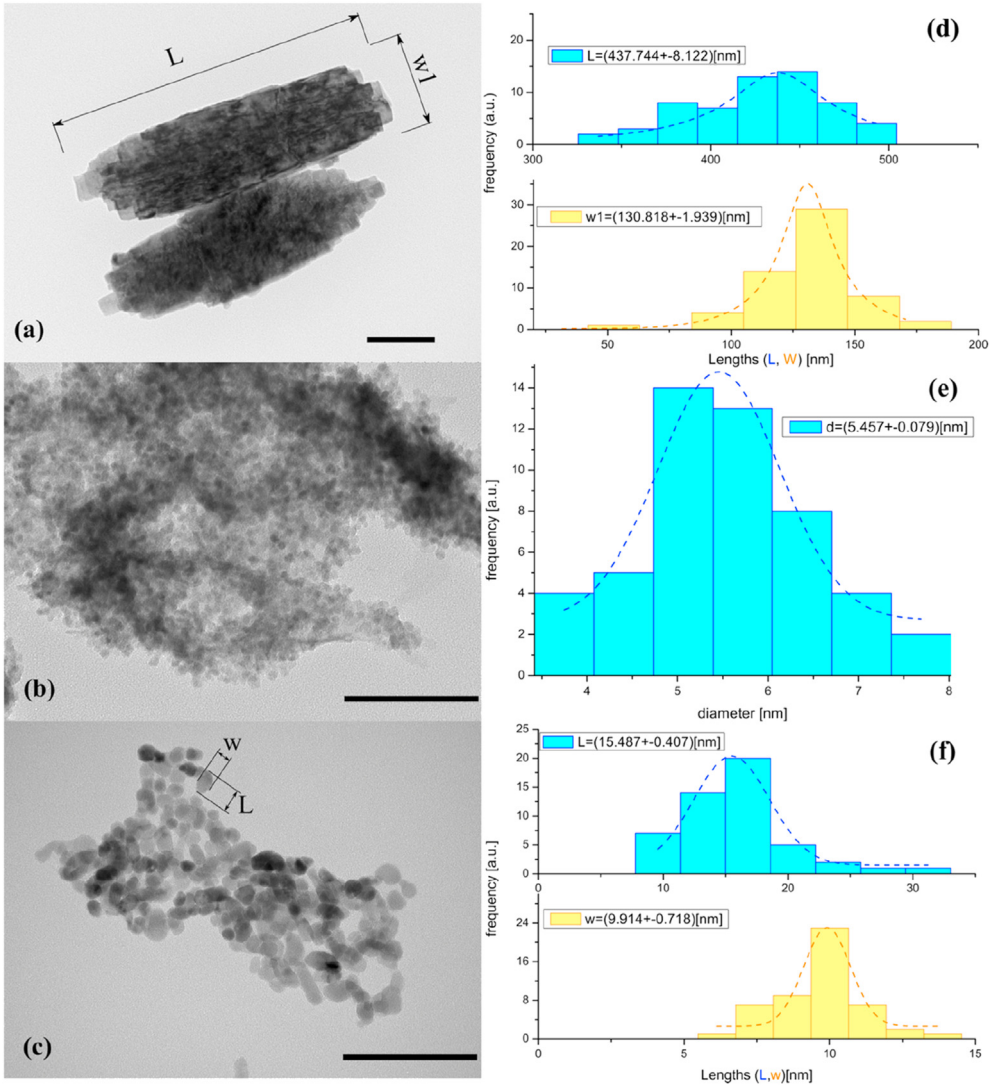

Figure 7. TEM images of ZnO structures obtained from synthesis: (a) I, (b) II and (c) III. All dimensions bars represent 100 nm length. Histograms of ZnO from synthesis: (d) I, (e) II and (f) III, according to every micrograph.

TEM image of ZnO structures obtained from synthesis II (Figure 7 (b)) shows ZnO NPs with spherical morphology organized into a large agglomeration. The corresponding histogram shows the size distribution of these ZnO NPs, where predominant diameters are around 5 nm.

TEM image corresponding to synthesis III (Figure 7 (c)) shows ZnO NPs with variable morphology and size, in ellipsoidal shapes, with widths between 5-15 nm and lengths between 8-30 nm approximately, with the presence of some nanorods. In this case, agglomeration is less pronounced compared to the previous synthesis.

In order to elucidate how the hydrozincite precursor of synthesis III is transformed into nanoparticles, a sequence of TEM images was recorded before solvothermal treatment (see Figure S6 in supplementary data). At first some wrinkled overlapped hydrozincite layers were observed with g-C_3N_4/ZnO nanosheets resemblance [73]. Once the drying process was performed, the nanorods/nanoparticles mixing phase was observed, suggesting the transformation of hydrozincite layers. Then, solvothermal treatment yielded well-dispersed nanoparticles from the nanorods, reducing time, and avoiding multiple steps compared to synthesis II. According to the literature, the synthesis of ZnO NPs with many Zn^{2+} precursors and $(NH_4)HCO_3$ produce the hydrozincite phase, following a 100 °C drying process and calcination at 500 °C [74], therefore, the synthesis used here could be proposed as solvothermal treatment enhanced to produce ZnO NPs at low work temperatures.

3.5. Ultrasonic treatments – TEM characterizations

With the aim to disaggregate possible nanostructures assembled from ZnO microstructures obtained by synthesis I, ultrasonic treatments were carried out on these micrometric ZnO samples dispersed in ethanol. Treatments consisted of undergo the samples to ultrasonic bath and also to ultrasonic probe for different times as the experimental section described.

With ultrasonic bath treatment, after 15 min it was observed that the microstructures remain but there are also spherical disaggregates. On a small scale, spherical nanoparticles with diameters ~20 nm were clearly identified together with surprising morphology comprising a central concavity or inner grill (see Figure S7.1; supplementary data). The sample treated for 30 min did not have an important percentage of breaking up and only a few structures in crumbling process were identified with diameters of 50 nm or more (see Figure S7.2; supplementary data). After 1 h of bath ultrasonic, no disaggregates were obtained, but it was possible to identify a hexagonal shape with sides of irregularly dimensioned between 20-45 nm (see Figure S7.2; supplementary data).

Smaller structures produced from the ultrasonic bath can probably be generated by an erosion process of the microstructure from the energy applied from ultrasound, promoting break up of some crystal planes yielding hexagonal layers and/or the polishing of micrometric structures

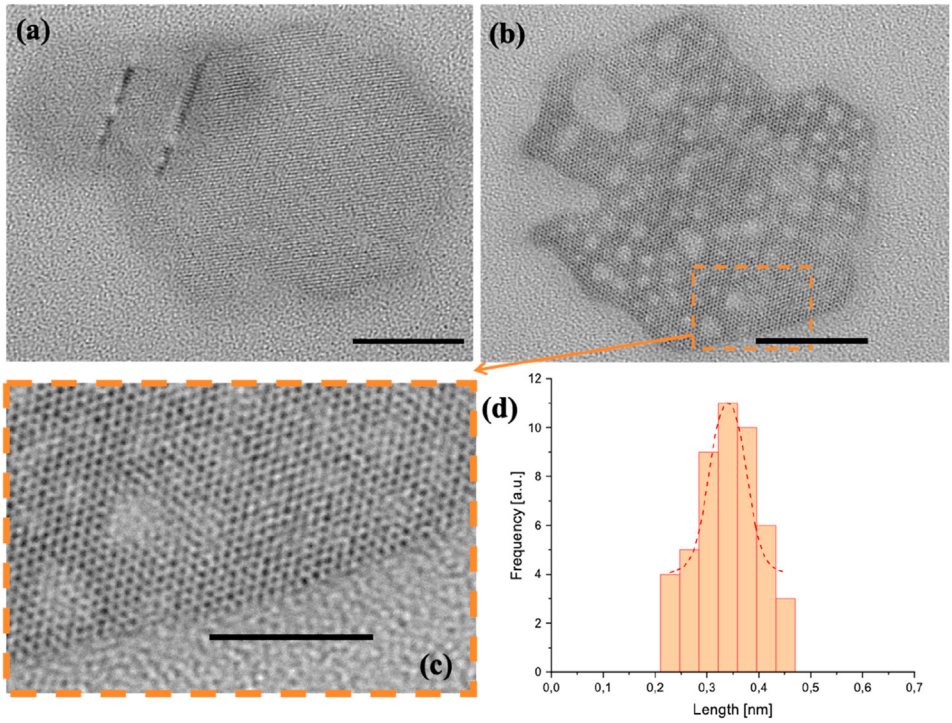

Figure 8. TEM images of ZnO hexagonal structures obtained from the synthesis I then of probe ultrasonic treatment for 30 min. Hexagonal plaquettes appear in (a), and these starts to break up when are exposed to the TEM electron beam (b). Before breakup, a porous structure in (c) with pore diameter close to 0.35 nm (d) was observed. Scale bars are 20nm (a-b) and 10nm (c).

to produce pseudospherical shapes. Apparently, more ultrasonic bathing time could generate disaggregation and agglomeration processes, without resulting in nanoparticles formation.

Using ultrasonic probe treatments for 30 min, microstructures remain but disaggregates of hexagonal porous nanoplates with sides ~28 nm of length are observed (Figure 8 (a, b)). The degradation of ZnO hexagonal nanosheet material was observed, when the material was exposed to the electron beam of TEM microscope, using an accelerated voltage of 120 kV for the electron beam, as shown in Figure 8b. Applying 60 min, porous laminar disaggregates without defined outlines were also observed and in the treated sample for 90 min, appear a clear hexagonal layer with 20 nm sides (Figure S7.3; supplementary data).

Figure 8 shows a TEM micrography of hexagonal nanoplates as a nanosheet containing nanopores of approximately 0.35 nm. This mesoporous material could be obtained by various methods of synthesis [75]. In our case the method employed comprises an economical precipitation synthetic route that leads into a mesoporous material enhanced with the combination of solvothermal treatment and ultrasonic irradiation processes, where the exfoliation of mixed ZnO microstructures leads to smaller nanoparticles with high porosity degree. Previous works have reported ZnO nanosized mesoporous materials made under different basic precipitation methods, using different zinc salts as the starting material, but most of them have a distinctive characteristic; the calcination process as the final stage [76, 77, 78], implying that high temperatures are responsible for the formation of these materials. The method described here differs from all of them by lacking a calcination process, but using ultra cavitation processes the same effect is accomplished, could be the predominant factor in the formation of mesoporous on ZnO surfaces. Therefore, this synthetic route couple to the ultrasonic process is a new and simple way to obtain mesoporous materials of ZnO, which is desirable for example in ultra-active photocatalysis [79], among other applications.

Similar to the ultrasound bathing, the processes carried out applying an ultrasonic probe device are also effective in exfoliating ZnO structures in smaller dimensions, from the microstructures produced by synthesis I. However, in the case of the probe, most of these disaggregates are obtained as nanoplates with hexagonal shapes and with significant inside porosity, which is attributed to the greater energy provided by this treatment compared to the bath [80, 81, 82, 83].

According to the results from ultrasonic treatments, in particular by the probe device, it is important to highlight the smaller structures obtained with a high degree of porosity since these cavities can serve as nanomaterials with a high surface reactivity, applied in antibacterial [84], photo remediation of heavy metals [85], inhibition of corrosion [86] or paper preservation [87].

4. Conclusions

ZnO NPs were synthesized under a precipitation method with a $ZnSO_4{\cdot}7H_2O$ source, enhanced with solvothermal treatment in ethylene glycol. The synthetic route that involves hydrozincite is reported for the first-time using potassium carbonate as a base and precipitating agent. Hidrozincite resulted to be an excellent intermediary in order to control the formation of nanosized zinc oxide material which resemblances a lamellar structure that is suitable to multi-step reactions that can lead to small, spherical and well defined nanostructures, under 200 °C solvothermal treatment. Furthermore, at low working temperature (<220 °C) hidrozincite is converted to mixed nano particles/rods phase, without the need of calcination processes, avoiding multiple reactions steps, shifting to disperse ZnO nanoparticles with mayor diameters, with ellipsoidal morphology under solvothermal treatment at 200 °C.

The synthetic route with $ZnSO_4{\cdot}7H_2O$ and NaOH ended up with micrometric ZnO structures. Ultrasonic irradiation is responsible to create an exfoliation degree from ZnO microstructures, resulting in mesoporous nanoparticles with hexagonal and circular morphologies exhibiting small nanoporous with grid fashion all over all over the nanoparticle surface. These structures could show surprising properties for future applications in biological, catalytic, energy conversion fields, among others.

In summary, ZnO NPs were obtained exclusively when ZnO was not formed during the initial precipitation step, therefore, ZnO NPs synthesis is highly dependent on pH. The strength of the base might be the driving force inducing/inhibiting hydrolysis and condensation reactions; being this factor essential to obtain a good size distribution.

Declarations

Author contribution statement

Daniel Navas: Conceived and designed the experiments; Performed the experiments; Analyzed and interpreted the data; Contributed reagents, materials, analysis tools or data; Wrote the paper.

Andrés Ibáñez: Performed the experiments; Analyzed and interpreted the data.

Iván González: Analyzed and interpreted the data; Contributed reagents, materials, analysis tools or data; Wrote the paper.

Juan Luis Palma: Performed the experiments; Analyzed and interpreted the data; Contributed reagents, materials, analysis tools or data; Wrote the paper.

Paulina Dreyse: Conceived and designed the experiments; Analyzed and interpreted the data; Contributed reagents, materials, analysis tools or data; Wrote the paper.

Funding statement

This work was supported by PI_M_2020_31 USM project, ANID (FONDECYT) Chile project numbers 11180185, 1201173 and 1201491, Projects CIP2018002 and CIP2018006 by Universidad Central de Chile and Basal Project AFB180001.

Data availability statement

Data included in article/supplementary material/referenced in article.

Declaration of interests statement

The authors declare no conflict of interest.

Additional information

Supplementary content related to this article has been published online at https://doi.org/10.1016/j.heliyon.2020.e05821.

References

[1] M. Ameri, M. Raoufi, M.R. Zamani-Meymian, F. Samavat, M.R. Fathollahi, E. Mohajerani, Self-assembled ZnO nanosheet-based spherical structure as photoanode in dye-sensitized solar cells, J. Electron. Mater. 47 (2018) 1993–1999.

[2] A.N.U. Haq, A. Nadhman, I. Ullah, G. Mustafa, M. Yasinzai, I. Khan, Synthesis approaches of zinc oxide nanoparticles: the dilemma of ecotoxicity, J. Nanomater. 2017 (2017) 8510342.

[3] J. Kwak, W.K. Bae, D. Lee, I. Park, J. Lim, M. Park, H. Cho, H. Woo, D.Y. Yoon, K. Char, S. Lee, C. Lee, Bright and efficient full-color colloidal quantum dot light-emitting diodes using an inverted device structure, Nano Lett. 12 (2012) 2362–2366.

[4] M.D. Marcantonio, S. Gellner, J.E. Namanga, J. Frohleiks, N. Gerlitzki, F. Vollkommer, G. Bacher, E. Nannen, Performance enhancement by ZnO nanoparticle layer in hybrid ionic transition metal complex-light-emitting electrochemical cells (iTMC-LECs), Adv. Mater. Technol. 2 (2017) 1600215.

[5] L. Qian, Y. Zheng, K.R. Choudhury, D. Bera, F. So, J. Xue, P.H. Holloway, Electroluminescence from light-emitting polymer/ZnO nanoparticle heterojunctions at sub-bandgap voltages, Nano Today 5 (2010) 384–389.

[6] S.P. Singh, S.K. Sharma, D.Y. Kim, Carrier mechanism of ZnO nanoparticles-embedded PMMA nanocomposite organic bistable memory device, Solid State Sci. 99 (2020) 106046.

[7] S.R. Khan, S. Abid, S. Jamil, A.I. Aqib, M.N. Faisal, M.R.S. AshrafJanjua, Layer by layer assembly of zinc oxide nanotubes and nanoflowers as catalyst for separate and simultaneous catalytic degradation of dyes and fuel additive, Chemistryselect 4 (2019) 5548–5559.

[8] M. Wang, A.-D. Li, J.-Z. Kong, Y.-P. Gong, C. Zhao, Y.-F. Tang, D. Wu, Fabrication and characterization of ZnO nano-clips by the polyol-mediated process, Nanoscale Res. Lett. 13 (2018) 47.

[9] N.A. Alshehri, A.R. Lewis, C. Pleydell-Pearce, T.G.G. Maffeis, Investigation of the growth parameters of hydrothermal ZnO nanowires for scale up applications, J. Saudi Chem. Soc. 22 (2018) 538–545.

[10] B. Bhushan, B.S. Murty, K. Mondal, A new approach for synthesis of ZnO nanorod flowerets and subsequent pure free-standing ZnO nanorods, Adv. Powder Technol. 30 (2019) 30–41.

[11] H.J. Jung, S. Lee, H.C. Choi, M.Y. Choi, Various shaped-ZnO nanocrystals via low temperature synthetic methods: surfactant and pH dependence, Solid State Sci. 21 (2013) 26–31.

[12] A. Kołodziejczak-Radzimska, T. Jesionowski, Zinc oxide—from synthesis to application: a review, Materials 7 (2014) 2833–2881.

[13] A. Šarić, I. Despotović, G. Štefanić, Solvothermal synthesis of zinc oxide nanoparticles: a combined experimental and theoretical study, J. Mol. Struct. 1178 (2019) 251–260.

[14] J. Medina, H. Bolaños, L.P. Mosquera-Sanchez, J.E. Rodriguez-Paez, Controlled synthesis of ZnO nanoparticles and evaluation of their toxicity in Mus musculus mice, Int. Nano Lett. 8 (2018) 165–179.

[15] X. Wang, Q. Zhang, Q. Wan, G. Dai, C. Zhou, B. Zou, Controllable ZnO architectures by ethanolamine-assisted hydrothermal reaction for enhanced photocatalytic activity, J. Phys. Chem. C 115 (2011) 2769–2775.

[16] J. Mayekar, S. Radha, V. Dhar, Role of salt precursor in the synthesis of zinc oxide nanoparticles, IJRET 3 (2014) 43–45.

[17] M. Gautam, M. Verma, G. Misra, Structural and optical properties of ZnO nanocrystals, J. Biomed. Nanotechnol. 7 (2011) 161–162.

[18] M.R.M. Sudha, Deactivation of photocatalytically active ZnO nanoparticle by surface capping with poly vinyl pyrrolidone, IOSR-JAC. 3 (2013) 45–53.

[19] R.H. Al-Dahiri, A.M. Turkustani, M.A. Salam, The application of zinc oxide nanoparticles as an eco-friendly inhibitor for steel in acidic solution, Int. J. Electrochem. Sci. 15 (2020) 442–457.

[20] Z. Ait Abdelouhab, D. Djouadi, A. Chelouche, L. Hammiche, T. Touam, Effects of precursors and caustic bases on structural and vibrational properties of ZnO nanostructures elaborated by hydrothermal method, Solid State Sci. 89 (2019) 93–99.

[21] X.-J. Huang, X.-F. Zeng, J.-X. Wang, J.-F. Chen, Transparent dispersions of monodispersed ZnO nanoparticles with ultrahigh content and stability for polymer nanocomposite film with excellent optical properties, Ind. Eng. Chem. Res. 57 (2018) 4253–4260.

[22] Y. Im, S. Kang, B.S. Kwak, K.S. Park, T.W. Cho, J.-S. Lee, M. Kang, Electrochemical performance of three shaped ZnO nanoparticles prepared in LiOH, NaOH and KOH alkaline solutions as anodic materials for Ni/Zn redox batteries, Kor. J. Chem. Eng. 33 (2016) 1447–1455.

[23] A. Katiyar, N. Kumar, A. Srivastava, Optical properties of ZnO nanoparticles synthesized by co-precipitation method using LiOH, Mater. Today 5 (2018) 9144–9147.

[24] A.M. Pourrahimi, D. Liu, V. Ström, M.S. Hedenqvist, R.T. Olsson, U.W. Gedde, Heat treatment of ZnO nanoparticles: new methods to achieve high-purity nanoparticles for high-voltage applications, J. Mater. Chem. A. 3 (2015) 17190–17200.

[25] Z.L.S. Seow, A.S.W. Wong, V. Thavasi, R. Jose, S. Ramakrishna, G.W. Ho, Controlled synthesis and application of ZnO nanoparticles, nanorods and nanospheres in dye-sensitized solar cells, Nanotechnology 20 (2008), 045604.

[26] M. Sessolo, H.J. Bolink, H. Brine, H. Prima-Garcia, R. Tena-Zaera, Zinc oxide nanocrystals as electron injecting building blocks for plastic light sources, J. Mater. Chem. 22 (2012) 4916–4920.

[27] M.T. Thein, S.-Y. Pung, A. Aziz, M. Itoh, The role of ammonia hydroxide in the formation of ZnO hexagonal nanodisks using sol–gel technique and their photocatalytic study, J. Exp. Nanosci. 10 (2015) 1068–1081.

[28] Z.M. Khoshhesab, M. Sarfaraz, Z. Houshyar, Influences of urea on preparation of zinc oxide nanostructures through chemical precipitation in ammonium hydrogencarbonate solution, Synth. React. Inorg. Met.-Org. 42 (2012) 1363–1368.

[29] M. Shamsipur, S.M. Pourmortazavi, S.S. Hajimirsadeghi, M.M. Zahedi, M. Rahimi-Nasrabadi, Facile synthesis of zinc carbonate and zinc oxide nanoparticles via direct carbonation and thermal decomposition, Ceram. Int. 39 (2013) 819–827.

[30] D. Francis, A. Abdub, S. Hendrik, B. Reinhardt, R. Kittesa, C. Liza, B. Mart, Optical properties of ZnO nanoparticles synthesized by varying the sodium hydroxide to zinc acetate molar ratios using a Sol-Gel process, Open Phys. 9 (2011) 1321–1326.

[31] A. Moezzi, M. Cortie, A. McDonagh, Aqueous pathways for the formation of zinc oxide nanoparticles, Dalton Trans. 40 (2011) 4871–4878.

[32] A. Šarić, I. Despotović, G. Štefanić, G. Dražić, The influence of ethanolamines on the solvothermal synthesis of zinc oxide: a combined experimental and theoretical study, Chemistryselect 2 (2017) 10038–10049.

[33] M. Mahendiran, A. Asha, J. Madhavan, M. Victor Antony Raj, Structural and optical analysis of 1D zinc oxide nanoparticles synthesized via hydrothermal method, Mater. Today 8 (2019) 412–418.

[34] N.M. Shamhari, B.S. Wee, S.F. Chin, K.Y. Kok, Synthesis and characterization of zinc oxide nanoparticles with small particle size distribution, Acta Chim. Slov. 65 (2018) 578–585.

[35] Y. Wang, J. Yang, J. Kong, H. Jia, Z. Wang, H. Jin, M. Yu, Synthesis of radial-like ZnO structure by hydrothermal method with $ZnSO_4{\cdot}7H_2O$ and $Zn(CH_3COO)_2{\cdot}2H_2O$ as zinc sources, Cryst. Res. Technol. 50 (2015) 414–419.

[36] X. Bai, L. Li, H. Liu, L. Tan, T. Liu, X. Meng, Solvothermal synthesis of ZnO nanoparticles and anti-infection application in vivo, ACS Appl. Mater. Interfaces 7 (2015) 1308–1317.

[37] X. Chen, X. Jing, J. Wang, J. Liu, D. Song, L. Liu, Self-assembly of ZnO nanoparticles into hollow microspheres via a facile solvothermal route and their application as gas sensor, CrystEngComm 15 (2013) 7243–7249.

[38] T. Ghoshal, S. Biswas, M. Paul, S. De, Synthesis of ZnO nanoparticles by solvothermal method and their ammonia sensing properties, J. Nanosci. Nanotechnol. 9 (2009) 5973–5980.

[39] A. Anzlovar, K. Kogej, Z. Crnjak Orel, M. Zigon, Polyol mediated nano size zinc oxide and nanocomposites with poly(methyl methacrylate), Express Polym. Lett. 5 (2011) 604–619.

[40] R. Devaraj, K. Karthikeyan, K. Jeyasubramanian, Synthesis and properties of ZnO nanorods by modified Pechini process, Appl. Nanosci. 3 (2013) 37–40.

[41] H. Cui, H. Liu, J. Wang, X. Li, F. Han, R.I. Boughton, Sonochemical synthesis of bismuth selenide nanobelts at room temperature, J. Cryst. Growth 271 (2004) 456–461.

[42] S. Jia, D. Zhang, Y. Xuan, L. Nastac, An experimental and modeling investigation of aluminum-based alloys and nanocomposites processed by ultrasonic cavitation processing, Appl. Acoust. 103 (2016) 226–231.

[43] S.H. Khan, S.R.B. Pathak, M.H. Fulekar, Development of zinc oxide nanoparticle by sonochemical method and study of their physical and optical properties, AIP Conf. Proc. 1724 (2016), 020108.

[44] D.G. Shchukin, E. Skorb, V. Belova, H. Möhwald, Ultrasonic cavitation at solid surfaces, Adv. Mater. 23 (2011) 1922–1934.

[45] Z. Sharifalhoseini, M.H. Entezari, R. Jalal, Direct and indirect sonication affect differently the microstructure and the morphology of ZnO nanoparticles: optical behavior and its antibacterial activity, Ultrason. Sonochem. 27 (2015) 466–473.

[46] S. Daumann, D. Andrzejewski, M. Di Marcantonio, U. Hagemann, S. Wepfer, F. Vollkommer, G. Bacher, M. Epple, E. Nannen, Water-free synthesis of ZnO quantum dots for application as an electron injection layer in light-emitting electrochemical cells, J. Mater. Chem. C. 5 (2017) 2344–2351.

[47] M. Di Marcantonio, J.E. Namanga, V. Smetana, N. Gerlitzki, F. Vollkommer, A.V. Mudring, G. Bacher, E. Nannen, Green-yellow emitting hybrid light emitting electrochemical cell, J. Mater. Chem. C. 5 (2017) 12062–12068.

[48] H.-W. Huang, J. Liu, G. He, Y. Peng, M. Wu, W.-H. Zheng, L.-H. Chen, Y. Li, B.-L. Su, Tunable macro–mesoporous ZnO nanostructures for highly sensitive ethanol and acetone gas sensors, RSC Adv. 5 (2015) 101910–101916.

[49] Y.M.A. Mohamed, Y.A. Attia, The influence of ultrasonic irradiation on catalytic performance of ZnO nanoparticles toward the synthesis of chiral 1-substituted-1H-tetrazolederivatives from α-amino acid ethyl esters, Appl. Organomet. Chem. 34 (2020) e5758.

[50] S. Hata, K. Taguchi, K. Oshima, Y. Du, Y. Shiraishi, N. Toshima, Preparation of Ga-ZnO nanoparticles using microwave and ultrasonic irradiation, and the application of poly(3,4-ethylenedioxythiophene)-poly(styrenesulfonate) hybrid thermoelectric films, Chemistryselect 4 (2019) 6800–6804.

[51] B. Li, K. Zhou, Z. Chen, Z. Song, D. Zhang, G. Fang, NH_4F-assisted one-pot solution synthesis of hexagonal ZnO microdiscs for efficient ultraviolet photodetection, R. Soc. Open Sci. 5 (2018) 180822.

[52] M. Noman, M. Petru, J. Militky, M. Azeem, M.A. Ashraf, One-pot sonochemical synthesis of ZnO nanoparticles for photocatalytic applications, modelling and optimization, Materials 13 (2019) 1–19.

[53] S.S. Khitam, E.D. Alhtheal, J.B. Azhar, Effect of zinc oxide nanoparticles preparation from Zinc Sulphate ($ZnSO_4$) against gram negative or gram positive microorganisms in vitro, Iraqi J. Vet. Med. 42 (2018) 18–22.

[54] L. Yang, L. Xiang, Influence of the mixing ways of reactants on ZnO morphology, J. Nanomater. 2013 (2013) 289616.

[55] S. Luo, R. Chen, L. Xiang, J. Wang, Hydrothermal synthesis of (001) facet highly exposed ZnO plates: a new insight into the effect of citrate, Crystals 9 (2019) 552.

[56] D.H. Piva, R.H. Piva, M.C. Rocha, J.A. Dias, O.R.K. Montedo, I. Malavazi, M.R. Morelli, Antibacterial and photocatalytic activity of ZnO nanoparticles from $Zn(OH)_2$ dehydrated by azeotropic distillation, freeze drying, and ethanol washing, Adv. Powder Technol. 28 (2017) 463–472.

[57] M. Wang, Y. Zhou, Y. Zhang, S.H. Hahn, E.J. Kim, From $Zn(OH)_2$ to ZnO: a study on the mechanism of phase transformation, CrystEngComm 13 (2011) 6024–6026.

[58] D. Luković Golić, G. Branković, M. Počuča Nešić, K. Vojisavljević, A. Rečnik, N. Daneu, S. Bernik, M. Šćepanović, D. Poleti, Z. Branković, Structural characterization of self-assembled ZnO nanoparticles obtained by the sol–gel method from $Zn(CH_3COO)_2{\cdot}2H_2O$, Nanotechnology 22 (2011) 395603.

[59] E.A. Meulenkamp, Synthesis and growth of ZnO nanoparticles, J. Phys. Chem. B 102 (1998) 5566–5572.

[60] M.C. Hales, R.L. Frost, Thermal analysis of smithsonite and hydrozincite, J. Therm. Anal. Calorim. 91 (2008) 855–860.

[61] K. Handore, S. Bhavsar, A. Horne, P. Chhattise, K. Mohite, J. Ambekar, N. Pande, V. Chabukswar, Novel green route of synthesis of ZnO nanoparticles by using natural biodegradable polymer and its application as a catalyst for oxidation of aldehydes, J. Macromol. Sci. Pure Appl. 51 (2014) 941–947.

[62] G. Xiong, U. Pal, J.G. Serrano, K.B. Ucer, R.T. Williams, Photoluminesence and FTIR study of ZnO nanoparticles: the impurity and defect perspective, Phys. Status Solidi C 3 (2006) 3577–3581.

[63] P. Fageria, S. Gangopadhyay, S. Pande, Synthesis of ZnO/Au and ZnO/Ag nanoparticles and their photocatalytic application using UV and visible light, RSC Adv. 4 (2014) 24962–24972.

[64] M.L. Singla, M. Shafeeq M, M. Kumar, Optical characterization of ZnO nanoparticles capped with various surfactants, J. Lumin. 129 (2009) 434–438.

[65] R. Liu, B. Pei, Z. Liu, Y. Wang, J. Li, D. Liu, Improved understanding of the sulfidization mechanism in amine flotation of Smithsonite: an XPS, AFM and UV–Vis DRS study, Minerals 10 (2020) 370.

[66] U.S. Rao, G. Srinivas, T.P. Rao, Influence of precursors on morphology and spectroscopic properties of ZnO nanoparticles, Proc. Mat. Sci. 10 (2015) 90–96.

[67] Z. Hu, G. Oskam, P.C. Searson, Influence of solvent on the growth of ZnO nanoparticles, J. Colloid Interface Sci. 263 (2003) 454–460.

[68] D.P. Joseph, C. Venkateswaran, Bandgap engineering in ZnO by doping with 3d transition metal ions, J. Atom. Molec. Opt. Phys. 2011 (2011) 270540.

[69] H. Che, J. Huso, J.L. Morrison, D. Thapa, M. Huso, W.J. Yeh, M.C. Tarun, M.D. McCluskey, L. Bergman, Optical properties of ZnO-alloyed nanocrystalline films, J. Nanomater. 2012 (2012) 963485.

[70] T.B. Ivetić, M.R. Dimitrievska, I.O. Gúth, L.R. Đačanin, S.R. Lukić-Petrović, Structural and optical properties of europium-doped zinc oxide nanopowders prepared by mechanochemical and combustion reaction methods, J. Res. Phys. 36 (2012) 43–51.

[71] J. Lian, Y. Liang, F.-l. Kwong, Z. Ding, D.H.L. Ng, Template-free solvothermal synthesis of ZnO nanoparticles with controllable size and their size-dependent optical properties, Mater. Lett. 66 (2012) 318–320.

[72] I. Danilenko, O. Gorban, P. Maksimchuk, O. Viagin, Y. Malyukin, S. Gorban, G. Volkova, V. Glasunova, M.G. Mendez-Medrano, C. Colbeau-Justin, T. Konstantinova, S. Lyubchyk, Photocatalytic activity of ZnO nanopowders: the role of production techniques in the formation of structural defects, Catal. Today 328 (2019) 99–104.

[73] P. Yang, J. Wang, G. Yue, R. Yang, P. Zhao, L. Yang, X. Zhao, D. Astruc, Constructing mesoporous g-C_3N_4/ZnO nanosheets catalyst for enhanced visible-light driven photocatalytic activity, J. Photochem. Photobiol., A 388 (2020) 112169.

[74] M. Pudukudy, Z. Yaakob, Simple chemical synthesis of novel ZnO nanostructures: role of counter ions, Solid State Sci. 30 (2014) 78–88.

[75] X.H. Huang, R.Q. Guo, J.B. Wu, P. Zhang, Mesoporous ZnO nanosheets for lithium ion batteries, Mater. Lett. 122 (2014) 82–85.

[76] R. Chen, J. Wang, L. Xiang, Facile synthesis of mesoporous ZnO sheets assembled by small nanoparticles for enhanced NO_2 sensing performance at room temperature, Sensor. Actuator. B Chem. 270 (2018) 207–215.

[77] Y. Xiao, H. Yu, X.-t. Dong, Ordered mesoporous CeO_2/ZnO composite with photodegradation concomitant photocatalytic hydrogen production performance, J. Solid State Chem. 278 (2019) 120893.

[78] H. Maltanava, S. Poznyak, E. Ovodok, M. Ivanovskaya, F. Maia, A. Kudlash, N. Scharnagl, J. Tedim, Synthesis of ZnO mesoporous powders and their application in dye photodegradation, Mater. Today 5 (2018) 17414–17421.

[79] N. Tripathy, R. Ahmad, H. Kuk, Y.-B. Hahn, G. Khang, Mesoporous ZnO nanoclusters as an ultra-active photocatalyst, Ceram. Int. 42 (2016) 9519–9526.

[80] N.N. Huy, V.T. Thanh Thuy, N.H. Thang, N.T. Thuy, L.T. Quynh, T.T. Khoi, D. Van Thanh, Facile one-step synthesis of zinc oxide nanoparticles by ultrasonic-assisted precipitation method and its application for H_2S adsorption in air, J. Phys. Chem. Solid. 132 (2019) 99–103.

[81] K. Su, J. Wu, D. Xia, Classification of regimes determining ultrasonic cavitation erosion in solid particle suspensions, Ultrason. Sonochem. 68 (2020) 105214.

[82] Y.-s. Kim, H. Rhim, M.J. Choi, H.K. Lim, D. Choi, High-intensity focused ultrasound therapy: an overview for radiologists, Korean J. Radiol. 9 (2008) 291–302.

[83] N.V. Dezhkunov, Investigation of sonoluminescence amplification under the interaction of ultrasonic fields widely differing in frequency, J. Eng. Phys. Thermophys. 76 (2003) 142–150.

[84] A. Gupta, R. Srivastava, Zinc oxide nanoleaves: a scalable disperser-assisted sonochemical approach for synthesis and an antibacterial application, Ultrason. Sonochem. 41 (2018) 47–58.

[85] P. Banerjee, S. Chakrabarti, S. Maitra, B.K. Dutta, Zinc oxide nano-particles–sonochemical synthesis, characterization and application for photo-remediation of heavy metal, Ultrason. Sonochem. 19 (2012) 85–93.

[86] S.B. Potdar, B.V.S. Praveen, S.H. Sonawane, Sonochemical approach for synthesis of zinc oxide-poly methyl methacrylate hybrid nanoparticles and its application in corrosion inhibition, Ultrason. Sonochem. 68 (2020) 105200.

[87] A.R.S. Majumdar, I. Nandi, P. Banerjee, S. Banerjee, M. Ghosh, S. Chakrabarti, Paper coated with sonochemically synthesized zinc oxide nanoparticles: enhancement of properties for preservation of documents, Tappi J. 17 (2017) 25–33.